Revisiting stress-oscillation in cold drawing of poly(ethylene terephthalate)

Ellen L. Heeley[a*], Jessica Smith[b], Chaoying Wan[b], Steven Huband[c], E. Brambley[d], Darren J. Hughes[e*]

[a] School of Life, Health and Chemical Sciences, The Open University, Milton Keynes, MK7 6AA, UK

[b] International Institute of Nanocomposites Manufacturing (IINM), WMG, The University of Warwick, CV4 7AL, UK

[c] Department of Physics, The University of Warwick, Coventry, CV4 7AL, UK

[d] Mathematics Institute. University of Warwick, Coventry CV4 7AL, UK

[e] WMG, The University of Warwick, Coventry, CV4 7AL, UK

* Corresponding authors: Ellen. L. Heeley, Ellen.Heeley@open.ac.uk and Darren J. Hughes, d.hughes@warwick.ac.uk.

Keywords: stress-oscillation, PET, thermography, small- and wide-angle X-ray scattering.

Abstract

This paper investigates the unusual phenomenon of stress-oscillation (SO) where a polymer exhibits periodic oscillatory neck propagation during drawing. It has been suggested that heat generation at the neck is critical, while other theories propose that an unstable neck stress is the controlling mechanism. Here, we study cold-drawing of poly(ethylene terephthalate) at 100 mm min^{-1} where SO has been monitored by thermal analysis. The morphology of the transparent and opaque bands were investigated using DSC, X-ray scattering and microscopy. It is revealed that heat release is a consequence of the plastic deformation as opposed to being the cause of the yielding. Neck geometry plays a key role in the mechanism. Temperature rise at the neck is low (9 ^{o}C) and does not lead to a change in crystalline morphology between the transparent and opaque bands. It is concluded that stress-induced crystallisation plays no role in the SO process for cold drawn PET and that the opaque bands result from axial voiding during high strain-rate yielding.

1. Introduction

A stress-oscillation (SO) phenomenon has been observed in several thermoplastic semi-crystalline polymers including poly(ethylene terephthalate) (PET) [1-9], high density polyethylene (HDPE), [7, 10] isotactic and syndiotactic polypropylene (iPP, sPP) [9, 11, 12] polyamide (PA) [7] and polybutylene succinate (PBS) [13, 14] during cold-drawing. The SO is observed as a non-constant stress during drawing. Resulting stress-strain curves of the polymer during SO show a characteristic periodic oscillation which is coupled with visible alternating opaque and transparent banding appearing in the necking section of the sample. However, this phenomenon occurs only under certain testing conditions (draw rate, geometry of sample and temperature [9]), being is observed in some thermoplastics and can be difficult to replicate.

Despite stress-oscillation being observed and reported for 20 years or more, it is still a poorly understood process. One of the most studied polymers undergoing stress-oscillation during cold drawing is PET. Early reports proposed that factors affecting SO behaviour in PET are strain rate, heat dissipation during necking and sample modulus of elasticity [15, 16].

The mechanism of SO, has often been proposed to implicate the conversion of mechanical work into thermal heat energy at the neck region of the polymer [17]. Indeed, a number of studies [2-4, 15, 18] on the cold drawing behaviour of PET have proposed that SO is controlled by heat release at the neck. One mechanism identified as a causal factor of SO is that strain energy during the drawing process results in heat increase allowing the molecular chains to soften, causing necking and creation of an oriented amorphous matrix. Toda [4] further pursued the impact of local heating on the SO mechanism, arguing that the heat increase drives the development of crystallinity, making the case that crystalline development accounts for the SO process. The case for crystallisation driving the SO process was also furthered by Kandilioti

[5], who studied SO samples via FTIR and Raman spectroscopy methods, making the case that the regions experiencing SO have increased crystallinity. Notably, their DSC data did not show increased crystallinity although it was stated that the DSC results lacked sensitivity for this type of measurement.

Karger-Kocsis [8] proposed a 'stick-slip' model to explain the SO behaviour during cold drawing of PET. Within the 'stick' phase, strain hardening occurs as a result of crystallisation, with the proceeding 'slip' phase leading to heat release. It was asserted that a stress-induced crystallisation process (SIC) drives localised crystallinity increase and results in opaque bands with a higher percentage crystallinity. However, it was suggested that the transparent bands were not crystalline. The paper makes the case that SO is only possible in polymers that are crystallisable. By consequence, the opaque (higher crystallinity) bands would correlate to the 'stick' phase (increasing load) and the transparent ones to the 'slip' phase (load release).

Significant localised temperature increases have been reported by some authors whereby the heat increase is often above T_g, supporting the argument of the necking process inducing crystallization. Toda [4] reports a temperature increase of up to 80 °C during cold drawing of PET, although the strain rate leading to this increase is 1000 mm min^{-1}. At lower strain rates, significantly smaller thermal changes are observed, whilst SO still occurs. Whilst Toda argued that creation of localised crystallinity controls the SO process, limited experimental evidence is provided to support any change in crystallinity. Indeed, experimental evidence for increased crystallinity in SO regions is scant in the literature. Ronkay [19] links opacity (from cavitation) with increased crystallinity but the link is unsupported experimentally. Ronkay makes further observations on cavitation timing with respect to the stress behaviour and argued that cavitation occurs prior to the sudden drop in stress and is not a direct cause of the stress release.

Finally, Pakula [1] departs from a causal link between localised heating and the origins of the SO process. They focussed on the neck critical stress as being the key driving mechanism for SO and argue that heat played no direct role.

In this paper, we focus on the SO behaviour of cold drawn PET and bring together a number of advanced analytical tools to provide a new insight into the SO mechanisms. We attempt to address several as yet unanswered questions. This includes investigating the detail of the cyclic stress and the correlated thermal behaviour, and obtaining a more complete understanding of the morphological differences between the undrawn and banded (opaque and transparent) PET material. The timing of the onset of transparent and opaque bands with respect to the oscillating stress field and the thermal response remains in debate in the literature which we will address. Importantly we will also investigate the correlations drawn by different authors between heat and final crystallinity, and link this to the SO behaviour.

2. Experimental

2.1 Materials and Sample Preparation

Commercial PET pellets (Arnite® A02 307, DSM) were dried in a desiccator oven at 130 ºC for approximately 12 hours to reach a moisture content of < 50 ppm. The PET films were prepared through a twin-screw extruder (L/D = 16) with processing profile of 260, 270, 250 and 240 ºC from the feeding zone to the film die. The film die had slit dimensions of 50 mm in width and 100 µm in thickness. The extruded films were collected on film rollers.

2.2. Characterization and testing

Simultaneous tensile testing and thermography

Samples were prepared for testing using a modified ASTM D638 (type V) [20] dogbone geometry. The sample which was utilized for the simultaneous tensile-thermography testing had a total length of 120 mm. The width of the area held in the tensile testing grips was 9.5

mm. The parallel length of the central gauge was 70.8 mm and the gauge width was 5.1 mm. The thickness of the sample was measured via a micrometer before testing as 0.24 mm.

Tensile testing was performed using a laboratory-based Shimadzu AGS-X dual column universal testing machine, rated to 10 kN and equipped with a 10 kN load cell. Simple mechanically-actuated sample grips were used. Crosshead extension was recorded during elongation with a sampling rate of 100 Hz. Elongation was set at a nominal rate of 100 mm min^{-1}. The test was performed at ambient temperature (approximately 25 °C). For calculation of mechanical properties of the sample in the elastic region, load and crosshead extension data were converted to engineering stress and engineering strain based on the initial gauge cross-sectional area only. This was a valid assumption as significant necking only occurred post-yield. Following ISO 527-1 [21], the modulus should be calculated between a strain of 0.000 and 0.002. However, due to compliance of the testing machine frame a non-linear initial loading phase was seen and thus modulus was calculated between a strain of 0.002 and 0.004 in a linear elastic region.

Thermal data was collected simultaneously during the tensile testing of the sample using a Flir SC5200 infra-red camera. The camera had an active area of 320 × 356 pixels at a pitch of 30 μm and employed an Indium Antimonide (InSb) detector. Full thermal frames were collected at a rate of 10 Hz with an assumed emissivity of 0.94. The thermal camera was positioned near-perpendicular to the face of the sample during tensile testing as shown in Figure 1A. Figure 1B shows a PET sample drawn at 100 mm min^{-1}, illustrating the stress-oscillation region, which is banded in nature.
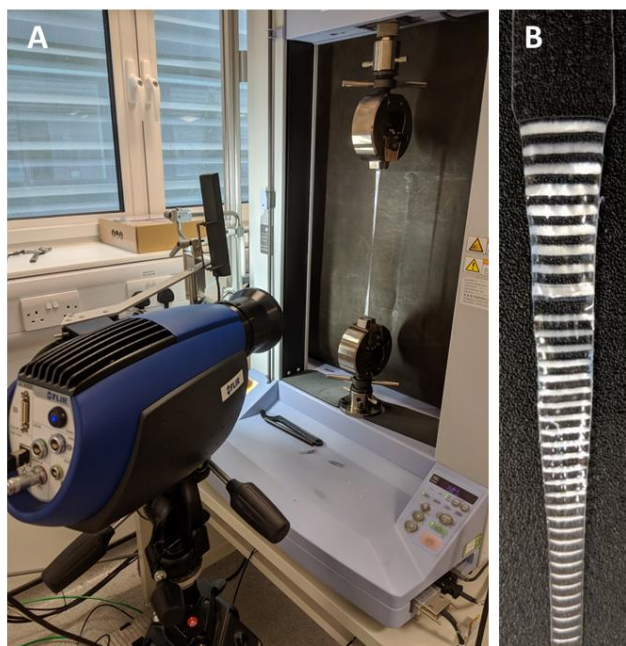
Figure 1 A: The Flir camera positioned next to the Shimadzu tensile testing machine for simultaneous collection of tensile and thermal data from PET samples. **B**: A section of PET sample drawn at 100 mm min^{-1} at ambient temperature showing banding from the neck.

The tensile data and the thermal data were not electronically synchronised. Both data sets were analysed following the experiment and were precisely synchronized using the point of sample rupture. The point of rupture was clearly identified at a single frame in the thermal data and could be correlated with a sudden drop in load data from the tensile testing machine. It is estimated that uncertainty in temporal alignment of the two data sets is no more than a single frame in the thermal data, i.e., estimated to be $\pm$ 0.05 s.

Polarized Optical Microscopy (POM) and Birefringence Imaging Microscopy (BIM)

A Zeiss Axio upright microscope was employed using polarized light in order to visualise a drawn sample. The sample used was not the same one as for tensile/thermal analysis but was drawn under the same conditions and exhibited stress oscillation. It should be noted that

whereas under unpolarised light, the opaque bands appear whitened, under polarized light, the white regions correlate to the transparent bands and dark regions to the opaque bands.

An Oxford Cryosystems Metripol was used for birefringence imaging microscopy (BIM) measurements of the drawn PET sample. This system consists of a rotatable linear polariser and a circular analyser and is described elsewhere [22]. The BIM instrument utilises a CCD detector containing 1360×1024 pixels. The method allows investigation of optical anisotropy ($|\sin\delta|$) which is sensitive to changes in both the birefringence and thickness of the material. The samples were aligned for BIM measurements such that the draw direction was near horizontal in the resulting images.

Differential scanning calorimetry (DSC) measurements

Differential scanning calorimetry (DSC) was performed on undrawn PET and cold drawn individual transparent and opaque bands using a Mettler Toledo DSC1 with STAR^e analysis software. Samples weighing 5 – 6 mg were heated between 0 ^{o}C and 300 ^{o}C and cooled to 0 ^{o}C at a rate of 10 ^{o}C min^{-1}. The glass transition temperature (T_g), melting temperature (T_m), cold crystallization temperature (T_{cc}), crystallization temperature (T_c), and degree of crystallinity ($X\%$) were determined from the DSC thermograms.

The degree of crystallinity X, for the undrawn PET and cold drawn transparent and opaque bands was calculated from Equation (1):

$$X = \frac{\Delta H_f}{\Delta H_f^0} \qquad\qquad\qquad \text{(Equation 1)}$$

Where ΔH_f is the enthalpy of fusion from the integrated area under the melting transition and ΔH_f^0 is the theoretical enthalpy change of 100% crystalline PET having a value of 140 J g^{-1} [23, 24].

Small- and-Wide angle X-ray scattering (SAXS/WAXS) measurements

X-ray scattering measurements were performed on undrawn PET and transparent and opaque bands from an as-drawn PET sample. The sample used was not the same one as for tensile/thermal analysis but was drawn under the same conditions and exhibited stress oscillation. To develop the crystalline oriented structure in the bands, the sample was annealed at 210 $^{\circ}$C. All X-ray measurements were performed on a Xenocs Xeuss 2.0 X-ray instrument operating with a Cu Kα source (λ = 1.54 Å) with a beam size of 500 µm × 500 µm. A section of the PET sample was clamped onto the heating block of a Linkam TST350 temperature controlled tensile testing stage which was then positioned horizontally in the instrument's evacuated sample chamber, as shown in Figure 2. The X-ray beam passed perpendicularly through the sample via a window in the heating block. The Linkam TST350 was located on a XYZ translation stage allowing positioning of the sample with respect to the beam. In this way diffraction was obtained from the transparent and opaque bands separately.
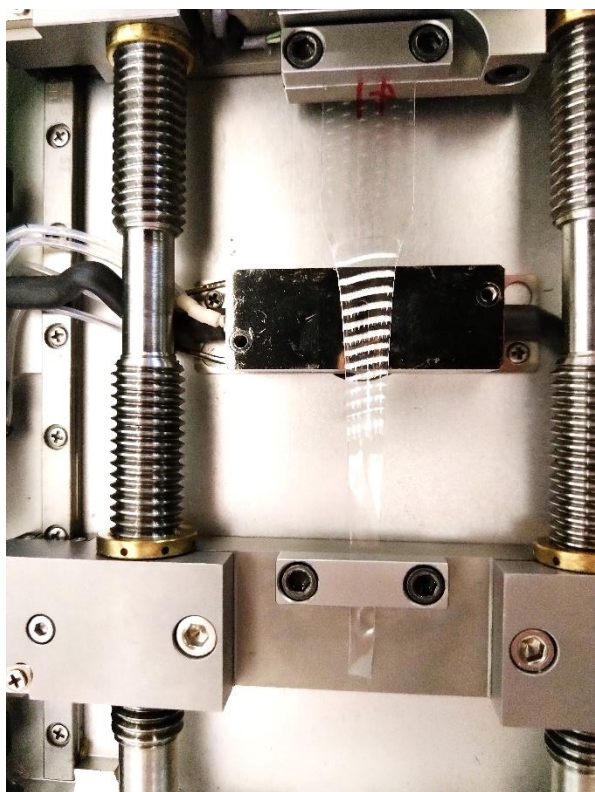
Figure 2 PET sample positioned in a Linkam TST350 tensile testing stage. A window obscured by the sample, is situated at the centre of the black heating block.

Simultaneous 2D small- and wide-angle X-ray scattering (2D SAXS/WAXS) patterns were captured on Pilatus 300 K and Pilatus 100 K detector systems respectively, which were calibrated using silver behenate. The SAXS detector was positioned at the end of an evacuated chamber to reduce air scattering, where the sample to detector distance was 1.2 m. The WAXS detector was positioned in the evacuated sample chamber at a sample-to-detector distance of 162 mm.

Each SAXS/WAXS pattern was collected over 120 seconds. The first SAXS/WAXS patterns were collected at 30 °C, which was the temperature in the sample chamber. Subsequently, the sample was heated to 210 °C at 20 °C min^{-1}, and held at this temperature for 120 seconds, then SAXS/WAXS patterns were collected for the transparent and opaque bands.

The 2D SAXS/WAXS patterns were normalized for sample thickness, transmission and background scattering using the Xeuss 2.0 instrument data processing and analysis software. Where necessary, the 2D SAXS/WAXS patterns were reduced to 1D scattering profiles of intensity I, versus scattering vector q, (where $q = (4\pi/\lambda) \sin(\theta)$) for SAXS and 2θ for WAXS. This was done for SAXS by integrating around the beam stop over the whole pattern, and for WAXS a sector integration was performed, given the available data, over the 2θ range of 18.5° to 47°.

3. Results

3.1 Mechanical performance of PET

Figure 3A, shows the full recorded load versus crosshead displacement for the PET dogbone sample that underwent simultaneous tensile-thermography testing. The data was recorded to sample failure at a displacement of approximately 240 mm (a video of the draw showing the oscillation is given in supplementary materials). The oscillation behaviour is seen to be globally unstable over much of the test but there are three distinct regions of oscillatory load. It is seen that once oscillation commences, the process appears stable until a point where conventional plastic elongation restarts. Figure 3B shows more detail of the first and second oscillatory regions. The sample draws in a normal elastic-plastic mode to approximately 95 mm when the first period of stress-oscillation commenced. Oscillation initially proceeded for a displacement of nearly 20 mm in total. Within this region of first oscillation there are two distinct regions. Firstly, a saw-tooth shaped load-extension region where the amplitude of oscillation was approximately 7−9 N and with a periodicity of approximately 1.8 mm. This was followed by a region of simpler sinusoidal-type oscillation with an amplitude of 1 N and a periodicity of approximately 1.0 mm. Within both regions of oscillation shown in Figure 3B it is observed that average load gradually increases. This can be explained by the observation that the

oscillating neck region progresses into the shoulder of the test piece i.e. the width of the neck increases.

The end of the first period of oscillation is marked by a sudden drop in load followed by a short period of simple plastic deformation. At 120 mm displacement a second period of oscillatory load behavior commences, lasting for approximately 70 mm. At the start of this region, oscillation is sinusoidal-type followed largely by saw-tooth behaviour. The third, final region of oscillation commences from approximately 215 mm and persists effectively to sample failure.
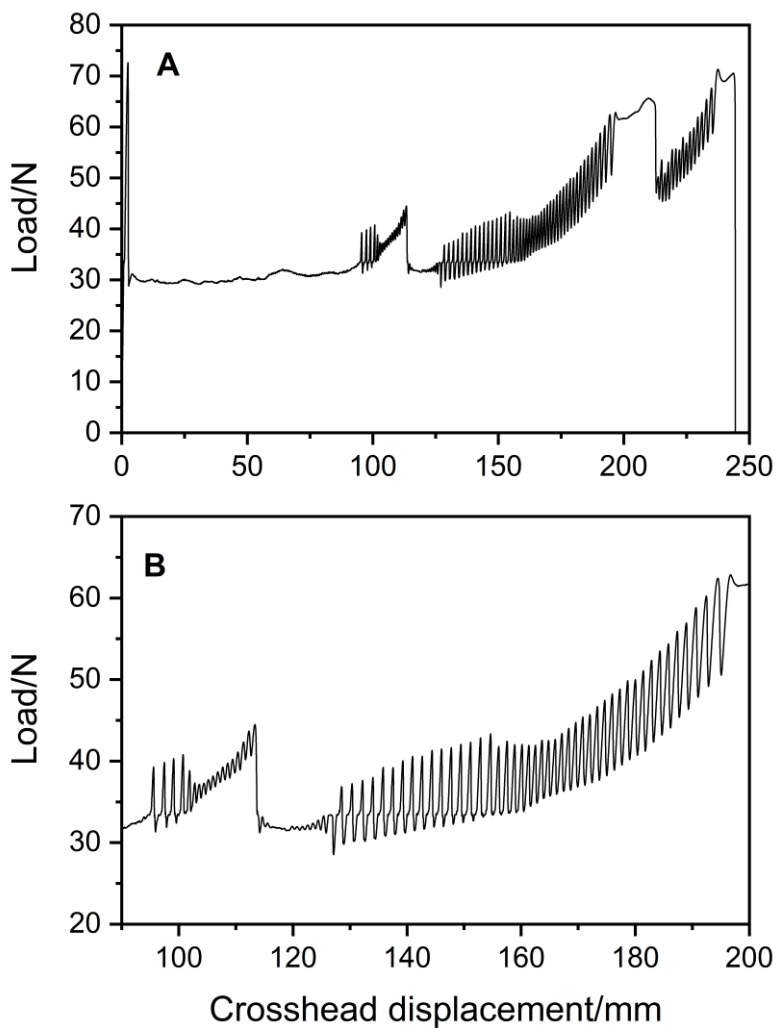
Figure 3 Load-extension curves for PET drawn at 100 mm min^{-1} at ambient temperature. **A**: Full load-extension data set showing three distinct regions of oscillatory behaviour. **B**: Load extension curve focused on the first and second oscillatory periods.

Figure 4, shows detail of the stress behaviour during the second phase of oscillation. Two stress cycles are presented revealing the detail of the stress-oscillation. Repeatability from cycle to cycle is excellent. The length of one repeat cycle is approximately 0.024 strain, corresponding to an elongation of approximately 1.80 mm. The figure shows regions of the stress-oscillation labelled from A to E. In zone A, a linear increase in stress is observed reaching a peak stress of approximately 32 MPa. This is followed by sample yield and rapid stress relaxation in zone B. Within zone B rapid sample elongation is observed at a local level (at the sample necking point). Zones C and D can be attributed to a shockwave in the sample due to the sudden stress unloading. This is followed by a period of slowly increasing stress in zone E prior to stiffening leading yet again to rapid yielding, and so on.
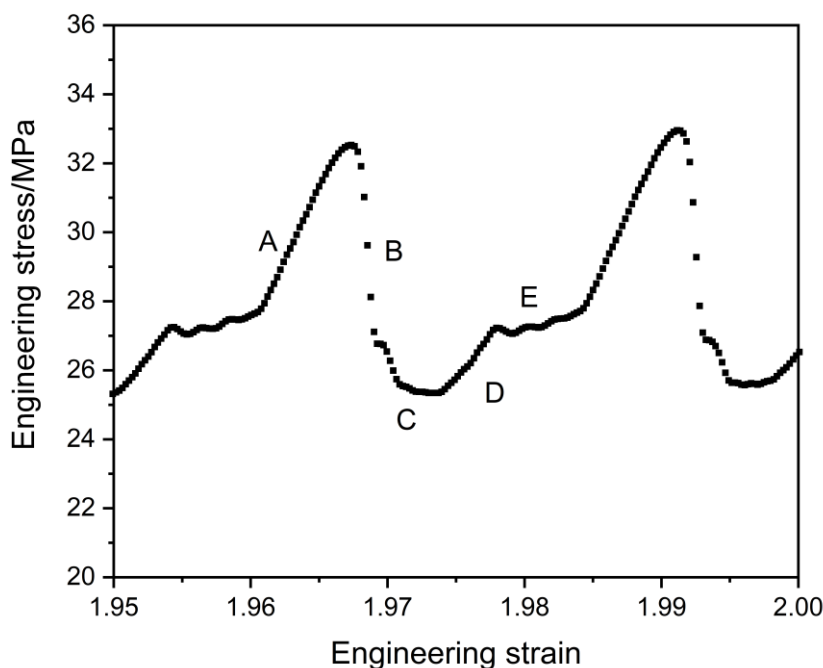
Figure 4 Stress-oscillation of PET drawn at 100 mm min^{-1} showing two cycles of oscillatory behaviour.

In order to calculate elastic modulus of the PET during elongation, the data presented in Figure 5, was fitted with a linear regression line resulting in a modulus of 2.70 ± 0.01 GPa which is in line with literature values for PET [25].
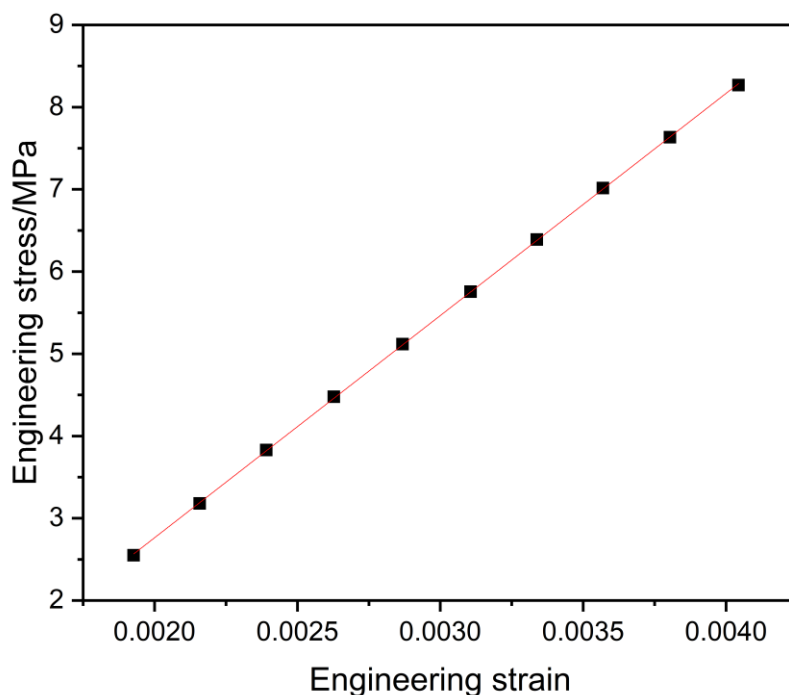

Figure 5 Engineering stress-strain response within the elastic region during the drawing of PET at 100 mm min^{-1} for calculation of elastic modulus.

3.2 Optical analysis of the SO region of PET

Figure 6A, shows the POM data of the magnified image of a PET sample drawn at 100 mm min^{-1} at ambient temperature with alternate discrete periodic bands of transparent and opaque material. The opaque (dark) bands have a thickness of approximately $200 - 250$ µm in comparison to approximately $300 - 400$ µm for the transparent (light) bands. Thus, the overall periodicity of the banding is approximately 0.5 mm. Note that these measurements are for the sample after removal from the test fixture i.e. unloaded. Closer inspection of the bands in Figure

6B (inset), shows that the transparent bands are characterised by a wrinkled pattern with the wrinkles extending perpendicular to the draw direction. Axial striations parallel to the draw direction are observed (Figure 6C) in the opaque bands, likely to be as a result of high strain-rate deformation associated with formation of the opaque bands. The thickness of the drawn region was measured to be between approximately 0.09-0.10 mm with no discernible difference between the opaque and transparent bands. This indicates that the absolute draw ratio of both transparent and opaque bands is similar. This is further supported by the X-ray scattering data presented in Section 3.4 where similar degrees of orientation are seen the drawn and annealed opaque and transparent bands.
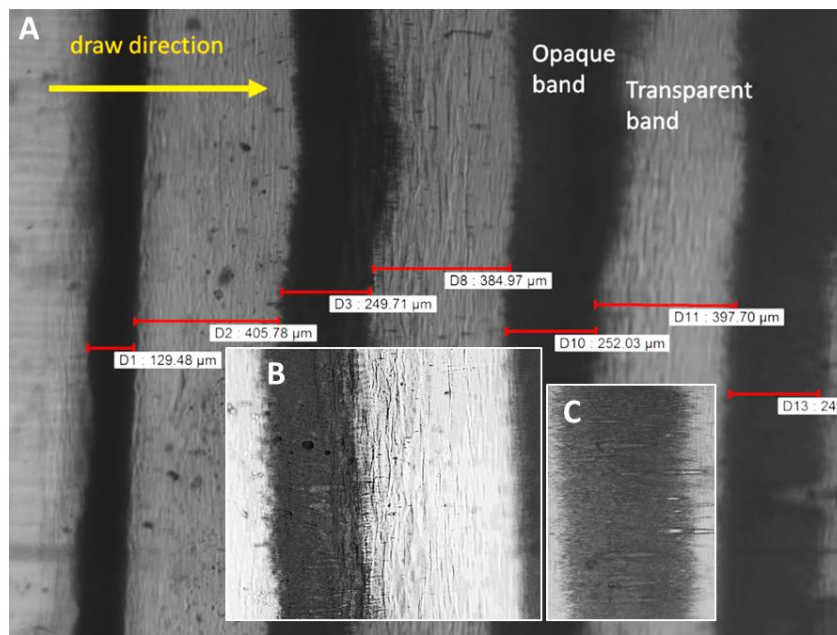
Figure 6 POM data for a PET sample drawn at 100 mm min⁻¹. **A**: magnified image of the PET with dimensions of the regular bands perpendicular to the draw direction (transparent bands light and opaque bands dark). **B**: inset - transverse wrinkling in the transparent band. **C**: inset - axial striations parallel to the draw direction in the opaque band.

Birefringence (BIM) data from a banded opaque-transparent region that originated during a stress-oscillation stage is shown in Figure 7. In the figure, the optical transmission image

(Figure 7A) is presented alongside the |sinδ| signal (Figure 7B). Similar to the POM data presented earlier, in the transmission data, the white regions represent the transparent bands and the dark regions the opaque bands. The BIM data show significant differences between transparent and opaque bands. The data reveals that the opaque bands display relative homogeneity in signal, not observed in the transparent bands. The transparent bands show interference stripes perpendicular to the loading direction. These bands correlate with the wrinkling described previously seen in the POM data (Figure 6B), and are likely a result of small changes in sample thickness perpendicular to the draw in the transparent bands. The absolute variation in |sinδ| in the transparent bands would correspond to a variation of approximately 0.006 mm. No such variation in thickness is seen in the opaque bands.
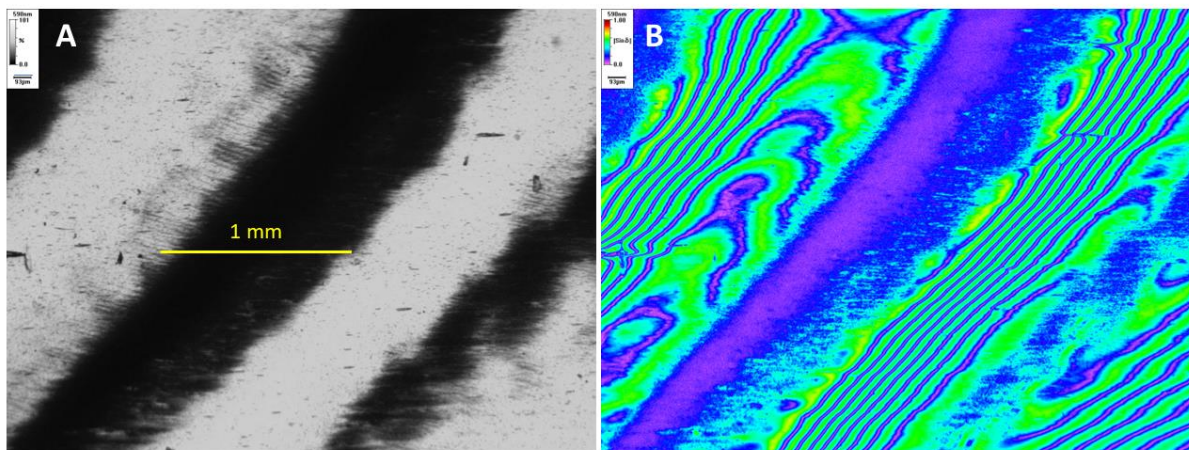

Figure 7 A: Transmission and **B**: |sinδ| images for a PET sample drawn at 100 mm min^{-1}. The images show a region of periodic transparent and opaque banding resulting during a stress-oscillation phase. The drawing axis is near-horizontal in the images.

3.3 Thermal analysis of undrawn and cold drawn PET

DSC was used to determine the thermal properties of the cold drawn PET stress-oscillation bands and compare these with the undrawn PET sample. Figure 8A and 8B, show the heat-cool DSC thermograms of the undrawn PET and of the cold drawn PET sample, respectively.

From Figure 8A, the glass transition temperature (T_g) of undrawn PET is seen at ~74 $^{\circ}$C. Furthermore, there is a clearly defined exotherm (T_{cc}), at ~131 $^{\circ}$C which is attributed to the cold crystallization process in the undrawn PET sample. However, in the thermograms for both the drawn transparent and opaque bands (Figure 8B) a cold crystallization peak is evident but is observed as a much broader exotherm. It is also seen that the T_g is at a lower temperature (~61 $^{\circ}$C). This broadening of T_{cc} and shift of T_g to lower temperatures has previously been seen for cold drawn PET [26-28], whereby this is due to the orientation of the molecular chains which then are more easily incorporated into a crystalline lattice. Some authors link this apparent absence of a T_{cc} peak to stress-induced crystallization (SIC), which had occurred during the cold drawing process [5, 29]. This is not the case here as the cold drawn PET SO bands did not show any significant crystallinity and from observing a broad T_{cc} in the DSC this indicates that crystallization does occur, but *only* during the DSC heating cycle. The observation that there is no significant and detectable crystallinity in the SO bands is confirmed later from X-ray data.
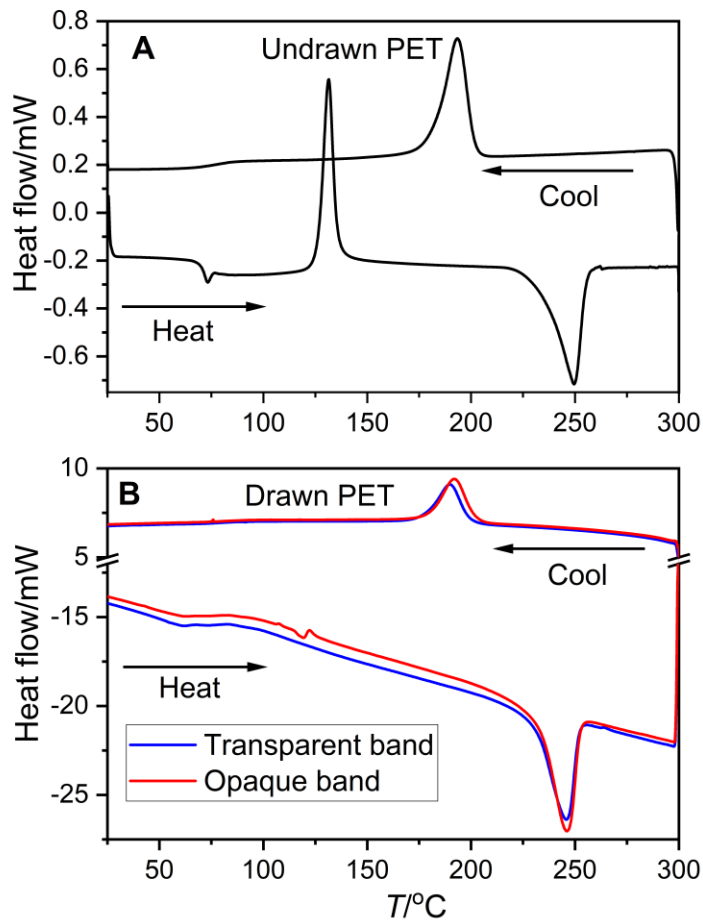
Figure 8　Heat-cool DSC thermograms of **A:** amorphous PET undrawn, and **B**: the individual transparent and opaque bands of cold drawn PET.

The thermal properties obtained from the thermograms in Figure 8, are presented in Table 1. The melting point (T_m) of the undrawn PET (after cold crystallization) is a little higher than that for the drawn transparent and opaque bands, but it is noteworthy to see that both the bands show no significant difference in T_m. Again, the value of T_c (on cooling) for the drawn transparent and opaque bands shows no significant difference (~2 ^{o}C).

The degree of crystallinity for the undrawn PET would be expected to be very low and can be obtained by subtracting the melting peak derived crystallinity (X_m) from the cold crystallization

crystallinity (X_{cc})[5], giving a value of 4.8%, indicating that the PET is indeed highly amorphous, but the small amount of residual crystallinity observed likely to be from the oriented chains from the initial processing, In contrast, the degree of crystallinity is increased significantly compared with the amorphous undrawn PET when the sample is cold drawn and has subsequently undergone the heating regime in the DSC instrument. However, from the DSC data the values of X_m for the transparent and opaque bands are almost the same with an average value of 37.5%. The increased value of X_m for both bands, compared with the undrawn PET, again shows that some crystallization has occurred during the DSC heating process, but the crystallinity of the bands is the same, indicating that the stress-oscillation process has no overall influence on the bulk crystallinity of the PET under these conditions. Further to this, the occurrence of the molecular orientation in the cold drawn PET transparent and opaque bands is confirmed using X-ray measurements.

Table 1. Thermal properties of PET stress-oscillation bands. Note X_{cc} and X_m represent the crystallinity from the cold crystallization peak and melting peak, respectively.

Sample	T_{cc}/°C	X_{cc}/%	T_c/°C	T_m/°C	X_m/%
Undrawn PET	131.6	25.5	193.4	249.5	30.3
PET transparent band	-	-	189.5	245.3	38.4
PET opaque band	-	-	191.5	246.1	36.6

3.4 SAXS/WAXS analysis of the opaque and transparent bands formed after drawing and after step annealing.

Figure 9, shows the 2D SAXS/WAXS patterns of the undrawn sample and transparent and opaque PET bands of the drawn sample. The SAXS/WAXS data was collected at 30 °C (the ambient temperature of the X-ray chamber) and after annealing at 210 °C. From the 2D SAXS patterns of undrawn PET at 30 °C, there is little scattering observed, indicating no long-range

order is present in the polymer. However, with the drawn opaque sample at 30 °C, there is a marked difference in the scattering around the central beamstop. In the opaque band sharp equatorial streaks are present perpendicular to the draw direction, which persist in the pattern after annealing at 210 °C. However, these central streaks are not observed in the SAXS of the transparent bands at 30 °C or 210 °C. The streaks can be attributed to the presence of voiding in the opaque bands and has been observed before in PET, sPP and PBS [8, 13, 14, 17, 19, 30] which showed similar stress-oscillation behaviour when drawn. The voids give rise to the opaque appearance or 'stress whitening' of the bands due to their size which scatters visible light. Here, SAXS is a common and important technique to be able to detect voiding and cavitation in semi-crystalline polymers, when drawn [31]. The equatorial scattering seen here in the PET opaque bands, indicates that the voids are elongated parallel to the draw direction.

Temp/°C	30	210
SAXS undraw		
WAXS undrawn		
SAXS Transparent band		
WAXS Transparent band		
SAXS Opaque band		
WAXS Opaque band		
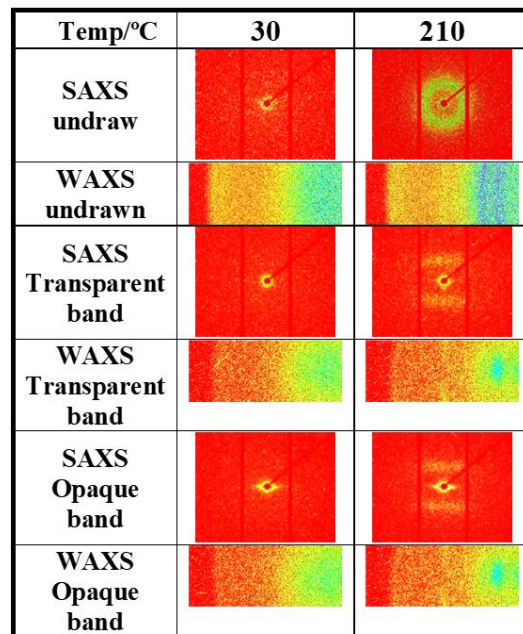
Figure 9 2D SAXS/WAXS patterns of undrawn PET and transparent and opaque bands of drawn PET at 30 °C and after annealing at 210 °C. The draw direction is vertical in all patterns.

Once annealed to 210 °C, the SAXS pattern for the undrawn PET, shows a broad but well-defined unoriented scattering ring around the central beamstop indicating an unoriented

lamellar structure had developed. The 2D SAXS patterns for both the transparent and opaque PET bands also show the appearance of broad peaks with intensity parallel to the equator at 210 °C, which suggests a well-oriented fibril-lamellar type of structure had developed [32, 33] but no difference is observed in the crystalline structure of either transparent or opaque bands. To confirm this Figure 10A, shows the 1D SAXS profiles obtained for the opaque and transparent bands annealed to 210 °C. Here, the broad peak shows that the fibril-lamellar structure has an average crystalline and amorphous layer stack distance of approximately 112 Å. Again, there is no observable difference in this crystalline structure in either the opaque or transparent bands, indicating that the stress-oscillation process does not influence the evolution, on annealing, of an oriented fibril-lamellar crystalline morphology of the PET.
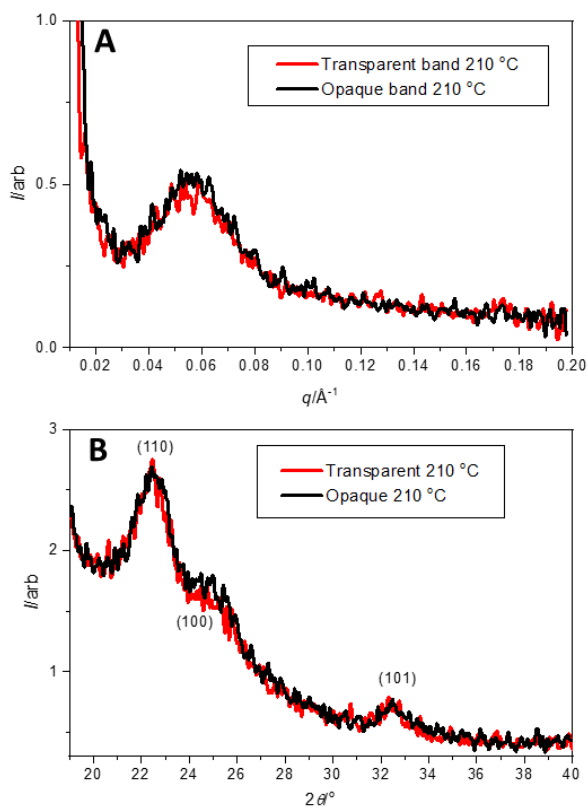
Figure 10 A: 1D SAXS and **B**: 1D WAXS profiles of PET transparent and opaque bands annealed at 210 °C.

To further confirm the crystalline structure development on annealing, 2D WAXS patterns were also recorded for the undrawn sample and opaque and transparent bands of the drawn PET, as shown in Figure 9. The 2D WAXS of the undrawn PET at 30 °C, shows a broad unoriented amorphous scattering peak, but at 210 °C clear Bragg rings are observed (indexed as the (110) and (100) of the triclinic PET unit cell crystal structure [34]), indicating an unoriented crystalline structure has developed. At 30 °C, the 2D WAXS for both the drawn transparent and opaque bands shows a broad peak of scattering intensity, which is attributed to oriented amorphous molecular chains. Once annealed an observable crystalline structure starts to develop and the Bragg peaks of PET start to emerge in the patterns. This is apparent in the 1D WAXS profiles in Figure 10B, where on annealing at 210 °C, the (110), (100) and (101) peaks of the triclinic unit cell crystal structure are observed [34]. It is important to note that the 2D WAXS data (Figure 9) of the PET shows no discernible crystalline structure, after cold drawing at 30 °C, which is confirmed in Figure 11. Here, the 1D WAXS profiles of undrawn amorphous PET and cold drawn PET transparent and opaque bands at 30 °C are shown.
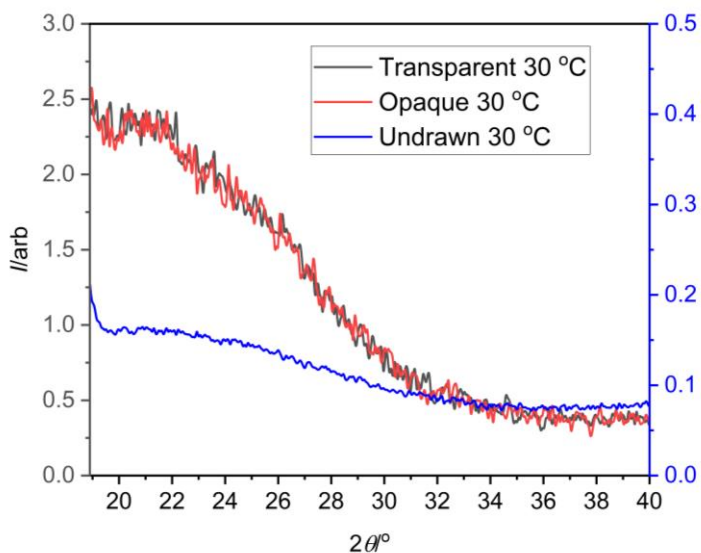
Figure 11 1D WAXS profiles of undrawn PET, and cold drawn PET transparent and opaque bands at 30 °C.

From Figure 11, it is evident that the undrawn PET shows a broad peak corresponding to an amorphous structure with no crystalline peaks evident. The transparent and opaque bands also show a broad peak but with a higher intensity which is due to the increased orientation of the amorphous structure due to drawing. Again, no crystalline peaks are observed. This indicates that the stress-oscillation process does not produce any significant stress-induced crystalline structure during cold drawing of PET, contrary to other reports [8, 16, 29]. This observation aligns to other X-ray studies focussing on cold drawn PET where below T_g an oriented amorphous structure is formed and only on annealing above T_g does any oriented well-defined crystalline structure develop [28, 35, 36].

In summary, the WAXS data at 30 ^{o}C, shows that oriented molecular chains are produced in both transparent and opaque bands. However, in the SAXS for the opaque bands, equatorial scattering streaks are observed indicating that voiding in the direction of the draw is also formed, which is absent in the transparent bands. On annealing, the combined SAXS/WAXS shows an oriented fibril-lamellar type of structure, which is comparable in both the opaque and transparent bands.

3.5 Thermography data during stress-oscillation process

Full-frame thermal data was collected throughout the sample deformation described in Section 3.1. The thermal data allowed investigation of any change in temperature at the drawing front and the links between thermal behaviour and the mechanically observed stress-oscillation. Figure 12, shows two full-frame thermal images from the thermal camera during the drawing of the PET sample. Figure 12A, shows the PET sample within the mounting grips before the sample elongation commenced. Figure 12B, shows an image during the second period of stable oscillation identified earlier in the mechanical data description. During the stable stress-oscillation phase a thermal spike is observed at the necking region of the sample. The intensity

of the thermal spike is visually seen to oscillate with time (and therefore crosshead displacement).
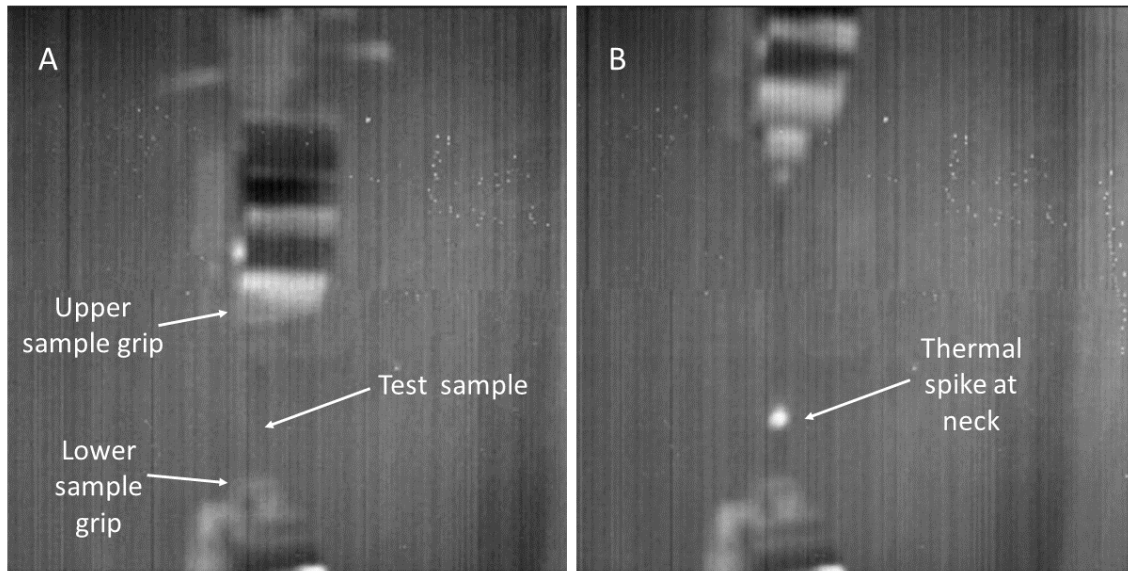

Figure 12 Full thermal images captured by the thermal camera for PET drawn at 100 mm min^{-1} at ambient temperature. **A**: Sample mounted in grips before commencement of elongation. **B**: Sample during elongation showing the thermal spike at the necking region.

In order to investigate the rise in temperature at the neck region, the thermal data was interrogated during the second period of oscillation i.e. matching the mechanical stress-oscillation data presented in Figure 4. Using the Research IR software package from Flir [37], a single line ROI (Region of Interest) was defined, oriented along the axis of the sample. The resulting line sampled the thermal profile along the section of the neck of the sample with a sampling width of 1 pixel and a length of 34 pixels. A single line ROI data set is shown in Figure 13, correlating to a maximum point (highest temperature) in the thermal cycle. The figure shows the temperature recorded along the length of the line ROI. It is important to note that the line ROI is taken from the undeformed material (low pixel number) to the deformed material (high pixel number). Whilst the data recorded by the thermal camera essentially

captures the surface temperature, with the thickness of the sample being only 100 µm in its drawn state, it is an appropriate assumption that the surface temperature is a good indicator of the internal temperature. From Figure 13, either side of the neck region, the material remains at ambient temperature (approximately 23 °C), whilst at the neck a maximum temperature increase of approximately 9 °C is observed. It is seen that once the material has necked and released heat, the temperature of the deformed material decays back to ambient. To understand the variation of temperature with time, the line ROI analysis above was repeated for all thermal image frames during a period of stress-oscillation. This was then presented as a thermal surface data plot, as shown in Figure 14. The figure shows the variation of temperature along the fixed line ROI over a period of two seconds during the second oscillation phase of sample elongation. The data relates to a similar region of the draw as is shown for the stress-oscillation detail in Figure 4. It is seen that the thermal profile follows a periodicity of approximately 1.0 − 1.2 seconds. The sample is seen to oscillate thermally, with the *hot-spot* located at the point of the necking of the dogbone. The position of the hotspot drifts towards a lower pixel value indicating that the neck progresses into the undrawn material. In summary, the sample is seen to release periodic thermal energy directly linked to the oscillatory nature of the stress response.
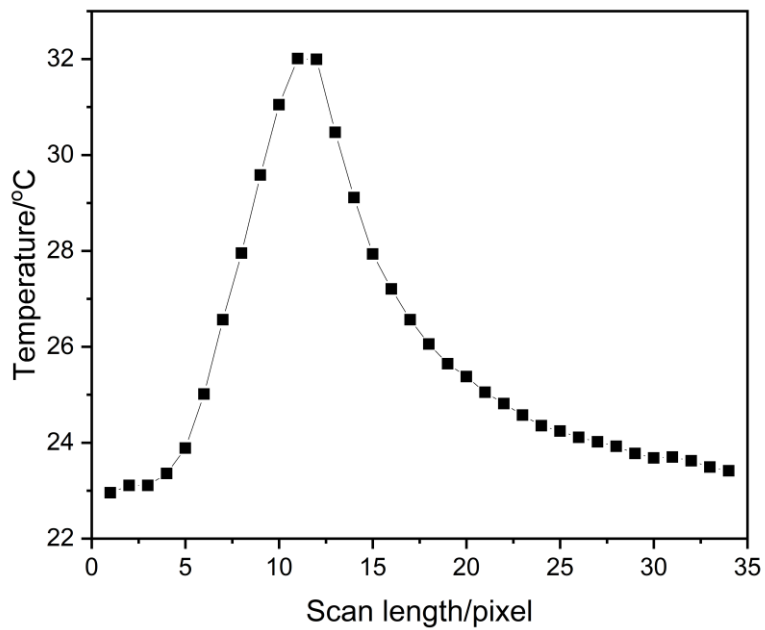
Figure 13 Line ROI showing the temperature distribution along the axis of the sample. The scan is 34 pixels in length, beginning from the undeformed region (low pixel number), through the necking front to the previously deformed material (high pixel number). A maximum temperature increase of 9 °C at the neck is seen.
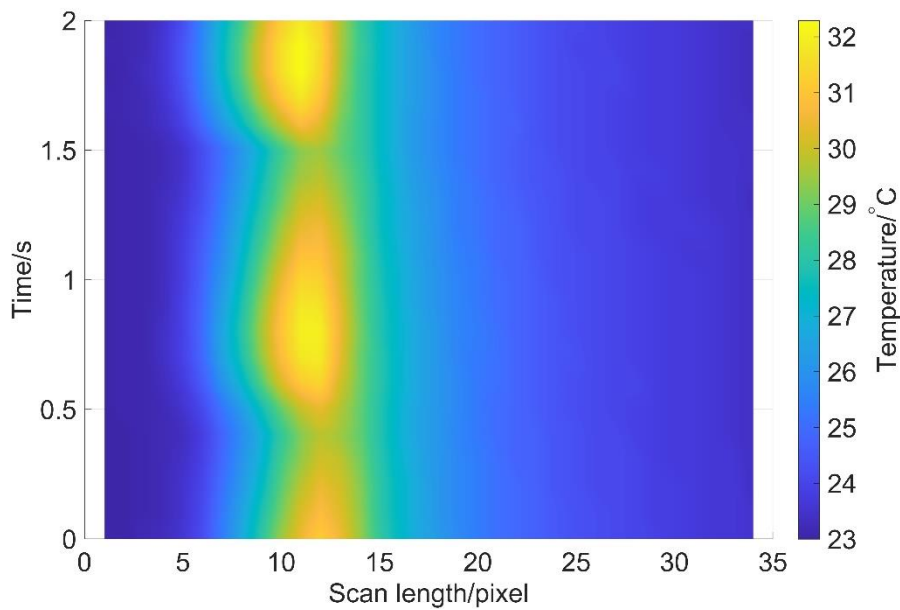
Figure 14 Thermal surface data during stress-oscillation of PET during drawing at 100 mm min^{-1}. The plot represents 2.0 seconds of thermal data along a fixed line ROI of 34 pixels in length, beginning from the undeformed region (low pixel number), through the necking front to the previously deformed material (high pixel number).

In order to investigate the relationship between oscillation of the mechanical and thermal data, the thermal output at the necking front was examined. This is relatively complicated to achieve because the neck itself moves relative to the thermal camera on each oscillation cycle. Thus to assess thermal output, a rectangular ROI was defined covering the whole region of the necking zone of the sample. In this way, a change in the average temperature within the rectangular ROI with time could be observed. Following the procedure described previously, the thermal data and the mechanical stress could be temporally aligned using the well-defined failure point of the sample. Figure 15, shows the temporally aligned mechanical load and average temperature within the rectangular ROI. The data presented specifically correlates with the mechanical data in Figure 4, but is more widely representative of the general thermal-load response during the three periods of oscillation.
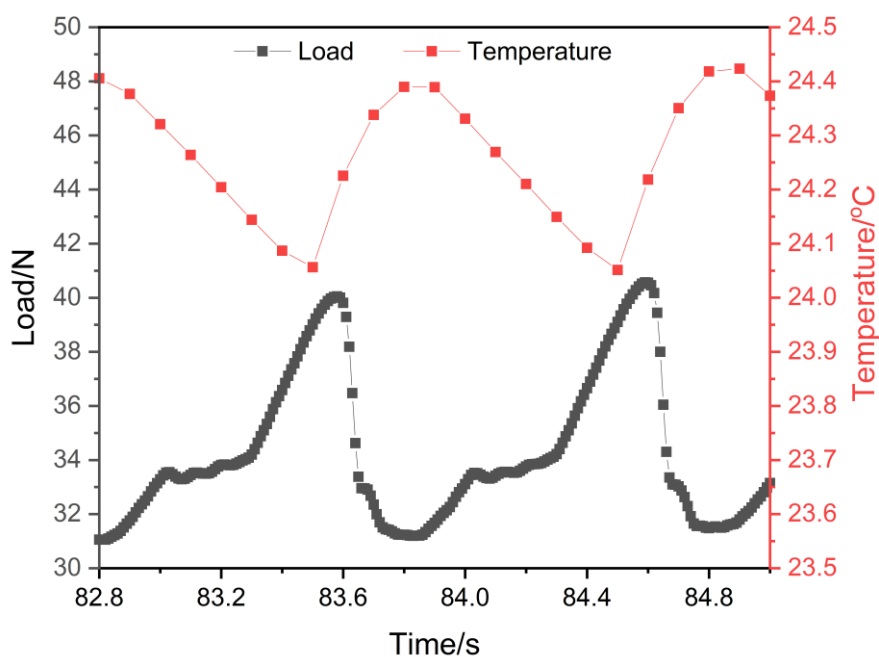
Figure 15 Temporally aligned mechanical load and thermal output data during drawing of PET at 100 mm min^{-1}. The load-temperature data is taken during the second period of oscillation and correlates to the mechanical data presented in Figure 4. The thermal data is an average temperature over the necking region of the sample, captured using a rectangular ROI. Uncertainty in temporal alignment (horizontal axis) of the load and temperature data sets is estimated to be no more than ± 0.05 s.

The data presented in Figure 15, is striking and presents an insight into the stress-oscillation observed in PET. Whilst other authors [4, 5] have claimed that increasing temperature during the sample loading phase leads to sample softening which in turn causes sample yielding, this is not supported by the data here. Conversely, during the elastic loading phase, the average sample temperature decreases. It is only at the point of yield that the temperature of the sample rises. The sample temperature rise is rapid and is correlated directly with the rapid yield. Linking to the data presented in Figure 13, the maximum rise in temperature seen at the sample neck was 9 °C. Immediately following the rapid yielding of the sample (i.e. during the shock wave phase), the sample begins to cool and this continues through the subsequent re-loading. The cyclic thermal behaviour has the same periodicity as the stress-oscillation. The data shows that strain energy accumulates during the loading phase and is released rapidly upon sudden sample yielding. Thus, the thermal release is a consequence of sample yielding rather than being causal to the yield.

4. Discussion and Conclusions

The study reported here provides an insight into the mechanisms of unusual oscillatory behaviour during cold drawing of PET. Similar behavior has been reported by a number of authors for various polymer systems although questions remain on the nature of the oscillation and its origins. This paper reports a detailed experimental campaign in order to gain an insight into the oscillatory stress behaviour.

It was shown that in a PET homopolymer sample drawn at a rate of 100 mm min^{-1} at 25 $^{\circ}$C (i.e. below T_g of PET), a regular stress-oscillation was observed at various stages of the draw (Figure 3). Initially, the sample was seen to draw elastically followed by yield and the formation of a stable neck. Following neck formation, the neck progressed initially in a steady manner at a constant stress. Three distinct zones of stress-oscillation were observed prior to sample fracture. The authors observed that whilst the stress-oscillation behaviour could be readily observed when drawing PET samples, its onset was unpredictable in nature. Often a sample would be observed to draw steadily until an unknown critical condition, possibly a localised imperfection, was reached. From the point oscillation commenced, it becomes highly repeatable after a number of cycles of increasing stress amplitude. The periods of stress-oscillation were observed over a highly variable strain range, with the oscillation appearing to reach some critical condition where oscillation ceases. In most cases, consecutive oscillation zones occurred in opposite sides of the drawing sample. Thus, the oscillating neck would cease, and the drawing front would translate from one side of the sample to the other, initially as a stable neck, until onset of a further period of oscillation. These observations indicate that neck geometry plays an important controlling role in the onset/offset of stress-oscillation. In this respect further work is underway to understand the physical drivers for stress-oscillation including sample geometry, neck form, temperature, mechanical properties and strain rate.

Inspection of the cold drawn PET sample showed that during steady-state elongation the sample remained in a transparent condition, similar to the undrawn state. However, upon entering a period of oscillation, the sample became banded in nature (Figures 6 and 7). Alternate discrete transparent and opaque bands were observed at a highly repeatable periodicity during the oscillation phase. In a post-experimental sample (relaxed) described

herein, opaque bands were approximately $200 - 250$ μm in length compared to approximately $300 - 400$ μm for the transparent bands i.e. approximately 0.5 mm periodicity.

Observed banding during oscillation can be directly linked to the saw-tooth stress pattern seen in Figure 4. The stress-strain pattern revealed several distinct zones which are linked to the formation of the sample banding. During the period of increasing stress, the sample draws in a steady state creating the transparent phase of the bands. The transparent material exhibits shear wrinkling perpendicular to the draw direction, presumably arising during the steady elongation process. At a peak stress condition (32 MPa in Figure 4), the sample suddenly yields, resulting in rapid elongation and the creation of an opaque band. During the unstable rapid yielding stage, voids are created and elongated, creating a whitened appearance (opaque bands). The process repeats as shown in Figures 3 and 4, resulting in a regular transparent-opaque banded visible structure.

The thermal imaging data was temporally linked to the stress data (Figure 15). The dominant feature of the thermal response is a rapid release of heat which coincides with rapid yielding in the sample neck, and which is due to release of stored strain energy. The sample then cools in the immediate post yield state. We thus correlate the formation of opaque bands directly with the high strain-rate yield and with the release of heat from the sample. This is interesting because previous authors [4] have attempted to explain the regular yielding during stress-oscillation to heat-build up and therefore sample softening i.e. the heat release during loading causes yielding. Here, we definitively show that heat release is caused by the sample starting to yield rather than being the cause of the onset of yield. In terms of absolute heat release at the point of yielding, data presented in Figures 13 and 14, show that a rise of no more than 10 ºC is seen in the sample tested. Discussion of temperature rise at this point is pertinent as several

authors [5, 8, 16, 19, 29] claim that the opaque bands produced during stress-oscillation is a result of localised stress-induced crystallisation (SIC). The case for SIC has been previously made in several ways. Firstly, that the opacity may indicate crystallinity, secondly that DSC data from opaque bands presents no cold crystallisation peak and thirdly that the heat from yielding could locally raise the temperature past T_g causing onset of crystallisation. In order to investigate this, the authors employed DSC and X-ray (SAXS/WAXS) diffraction on both transparent and opaque bands.

From the X-ray data of both transparent and opaque bands, it was observed that there was no significant difference between the two regions. In both regions, there is orientation observed in the amorphous ring (WAXS pattern), which has been induced during the drawing of the PET material. In both regions no crystalline peaks are apparent in the WAXS data. The SAXS data for the opaque bands exhibit equatorial scattering, corresponding to the existence of axially elongated voids [31] in the drawn sample; this is in contrast to the transparent bands where equatorial scattering is not present. Upon annealing of the transparent and opaque bands there is also no noticeable difference in attained crystallinity or oriented fibril-lamellar structure.

Differential Scanning Calorimetry (DSC) was used to further investigate the crystallinity in transparent and opaque bands. As noted previously, the X-ray data indicated a lack of any significant crystallinity in both the as-drawn transparent and opaque bands. This is however in contrast to assertions by other authors [5, 29], based on DSC data, that the transparent and opaque bands display significantly increased levels of crystallinity in comparison to undrawn material. This assertion is generally linked to SIC and an increased temperature in the neck region. The DSC data reported in this study is indeed similar to that reported in previous studies, although here we draw an alternative conclusion. Whilst the DSC data for undrawn PET, shows a well-defined cold-crystallization peak at approximately 130 °C, no such obvious peak exists in both drawn datasets. It is this feature that has led to previous assertions that SIC

during drawing means that any further cold-crystallization during DSC testing is limited. However, we believe that the drawn PET, both transparent and opaque, exhibit a wider cold crystallization feature commencing post T_g. The value of T_g was also lowered with respect to the undrawn PET. The early onset of cold crystallization in drawn PET samples can be attributed to the high degree of chain orientation, creating preferential nucleation sites during heating (by DSC). In combination with the X-ray data presented earlier, it is argued here that no stress-induced crystallinity is observed in the drawn samples. This is further supported by the observation that the temperature rise in the neck during drawing is merely around 10 °C above ambient. Thus, it can be concluded that after drawing, the transparent band is oriented but has no discernible crystalline structure (that is, a very low crystallinity) and that the opaque band is alike but with axially elongated voids (i.e. stress whitening) due to high-strain rate cold drawing.

The work presented here offers insight into the nature of the stress-oscillation in a drawn PET sample. The work brings together a range of experimental techniques for the first time which has enabled new conclusions on the links between the oscillatory stress behaviour, thermal characteristics and morphology of the banded regions. Whilst this paper reaches important conclusions on the effects of the stress-oscillation in PET, further work is now in progress by the authors to investigate the macro-molecular origins of the stress-oscillation via a modelling approach.

Conflicts of interest

There are no conflicts to declare.

References

[1] T. Pakula, E.W. Fischer, Instabilities of the deformation process in cold drawing of poly(ethylene terephthalate) and other polymers, Journal of Polymer Science: Polymer Physics Edition 19(11) (1981) 1705-1726.

[2] A. Toda, Oscillation and instability of neck propagation in poly(ethylene terephthalate) films, Polymer 34(11) (1993) 2306-2314.

[3] A. Toda, Oscillatory neck propagation in polymer films: 2, Polymer 35(17) (1994) 3638-3642.

[4] A. Toda, C. Tomita, M. Hikosaka, Y. Hibino, H. Miyaji, C. Nonomura, T. Suzuki, H. Ishihara, Thermo-mechanical coupling and self-excited oscillation in the neck propagation of PET films, Polymer 43(3) (2002) 947-951.

[5] G. Kandilioti, G.K. Govaris, V.G. Gregoriou, Vibrational Spectroscopic Study on the Origin of Stress Oscillation during Step-Wise Stretching in Poly(Ethylene Terephthalate), Applied Spectroscopy 58(9) (2004) 1082-1092.

[6] S.L. Bazhenov, L.I. Manevich, Criterion for neck-propagation stability in polymers, Polymer Science Series A 52(2) (2010) 168-174.

[7] S. Bazhenov, Y.A. Rodionova, K. As, Self-oscillation neck propagation in various polymers, Polymer Science Series A 45 (2003) 635-639.

[8] J. Karger-Kocsis, O.I. Benevolenski, E.J. Moskala, Toward understanding the stress oscillation phenomenon in polymers due to tensile impact loading, Journal of Materials Science 36(14) (2001) 3365-3371.

[9] H. Ebener, B. Pleuger, J. Petermann, Stress and strain oscillations in syndiotactic polypropylene and in poly(ethyleneterephthalate), Journal of Applied Polymer Science 71(5) (1999) 813-817.

[10] D.E. Mouzakis, J. Karger-Kocsis, Effects of gasoline absorption on the tensile impact response of HDPE/Selar™ laminar microlayer composites, Journal of Applied Polymer Science 68(4) (1998) 561-569.

[11] D. Mouzakis, Study of the stress oscillation phenomenon in syndiotactic polypropylene/montmorillonite nanocomposites, eXPRESS Polymer Letters 4 (2010) 244.

[12] M.C. García Gutiérrez, J. Karger-Kocsis, C. Riekel, Stress oscillation-induced modulated phase transformation and yielding in syndiotactic polypropylene, Chemical Physics Letters 398(1) (2004) 6-10.

[13] T. Wan, J. Zhang, S. Liao, T. Du, An investigation of stress oscillation in poly(butylene succinate-co-cyclohexanedimethylene succinate), Polymer Engineering & Science 55(4) (2015) 966-974.

[14] C. Wan, E.L. Heeley, Y. Zhou, S. Wang, C.T. Cafolla, E.M. Crabb, D.J. Hughes, Stress-oscillation behaviour of semi-crystalline polymers: the case of poly(butylene succinate), Soft Matter 14(45) (2018) 9175-9184.

[15] G. Andrianova, A. Kechekyan, V. Kargin, Self-oscillation mechanism of necking on extension of polymers, Journal of Polymer Science Part A-2: Polymer Physics 9(11) (1971) 1919-1933.

[16] R. Roseen, Temperature effect at self-oscillating necking during extension of polyethylene terephthalate (PETP), Journal of Materials Science 9(6) (1974) 929-933.

[17] S. Bazhenov, Self-oscillatory neck propagation in polymers, Journal of Applied Polymer Science 119(2) (2011) 654-661.

[18] G. Barenblatt, Self-oscillating neck propagation in polymers, Bulletin of the Russian Academy of Sciences: Mechanics of Solids 5 (1970) 110-118.

[19] F. Ronkay, T. Czigány, Cavity formation and stress-oscillation during the tensile test of injection molded specimens made of PET, Polymer Bulletin 57(6) (2006) 989-998.

[20] A. International, ASTM D638-14, Standard Test Method for Tensile Properties of Plastics, ASTM International2015.

[21] ISO, ISO 527-1:2019(en)

Plastics — Determination of tensile properties — Part 1: General principles, ISO, 2019, p. 26.

[22] A.M. Glazer, J.G. Lewis, W. Kaminsky, An automatic optical imaging system for birefringent media, Proceedings of the Royal Society of London. Series A: Mathematical, Physical and Engineering Sciences 452(1955) (1996) 2751-2765.

[23] H.W. Starkweather Jr., P. Zoller, G.A. Jones, The heat of fusion of poly(ethylene terephthalate), Journal of Polymer Science: Polymer Physics Edition 21(2) (1983) 295-299.

[24] B. Wunderlich, Thermal analysis of polymeric materials, Springer Science & Business Media2005.

[25] DSM, Arnite® A02 307 https://omnexus.specialchem.com/product/t-dsm-arnite-a02-307. (Accessed 02/02/ 2023).

[26] A. Bartolotta, G. Di Marco, F. Farsaci, M. Lanza, M. Pieruccini, DSC and DMTA study of annealed cold-drawn PET: a three phase model interpretation, Polymer 44(19) (2003) 5771-5777.

[27] Z. Zhang, S. Wu, M. Ren, C. Xiao, Model of cold crystallization of uniaxially oriented poly(ethylene terephthalate) fibers, Polymer 45(13) (2004) 4361-4365.

[28] U. Göschel, Thermally stimulated structural changes in highly oriented glassy poly(ethylene terephthalate), Polymer 37(18) (1996) 4049-4059.

[29] X. Wu, V.M. Tiwari, K.P. Suryarao, R. Tan, R. Xiao, H. Lv, Y. Zhang, Z. Wang, W.M. Huang, Patterned Colouring via Variable-Speed Single Stretching, Inventions 7(4) (2022) 93.

[30] M.G.a. Gutiérrez, J. Karger-Kocsis, C. Riekel, Stress oscillation-induced modulated phase transformation and yielding in syndiotactic polypropylene, Chemical physics letters 398(1-3) (2004) 6-10.

[31] Y. Lu, Y. Men, Cavitation-Induced Stress Whitening in Semi-Crystalline Polymers, Macromolecular Materials and Engineering 303(11) (2018) 1800203.

[32] E.L. Heeley, T. Gough, D.J. Hughes, W. Bras, J. Rieger, A.J. Ryan, Effect of processing parameters on the morphology development during extrusion of polyethylene tape: An in-line small-angle X-ray scattering (SAXS) study, Polymer 54(24) (2013) 6580-6588.

[33] S. Röber, P. Bösecke, H.G. Zachmann, Small angle X-ray scattering pole figures of semicrystalline polymers obtained by synchrotron radiation, Makromolekulare Chemie. Macromolecular Symposia 15(1) (1988) 295-310.

[34] R.D.P. Daubeny, C.W. Bunn, C.J. Brown, W.L. Bragg, The crystal structure of polyethylene terephthalate, Proceedings of the Royal Society of London. Series A. Mathematical and Physical Sciences 226(1167) (1954) 531-542.

[35] T. Asano, F.J. Baltá Calleja, A. Flores, M. Tanigaki, M.F. Mina, C. Sawatari, H. Itagaki, H. Takahashi, I. Hatta, Crystallization of oriented amorphous poly(ethylene terephthalate) as revealed by X-ray diffraction and microhardness, Polymer 40(23) (1999) 6475-6484.

[36] T. Asano, T. Seto, Morphological Studies of Cold Drawn Poly(ethylene terephthalate), Polymer Journal 5(1) (1973) 72-85.

[37] FLIR Thermal Studio Suite, 2022. https://www.flir.co.uk/products/flir-thermal-studio-suite/?utm_source=google&utm_medium=cpc&utm_campaign=emea.uk.solutions.cmvol.l.aw.om.thermalstudio.search&gclid=Cj0KCQjwjbyYBhCdARIsAArC6LKmExOluL7AP8l1V1GZDe0Apji7UzZmFQVJWfC0ac6HQRF7QQpfy5saAthTEALw_wcB. (Accessed 02/02/2023 2022).